AD

TECHNICAL REPORT ARCCB-TR-01025

COATING-BOND EVALUATION USING DISPERSION CURVES AND LASER-ULTRASONICS

AGOSTINO ABBATE
BRYON KNIGHT
MOAYYED A. HUSSAIN
JULIUS FRANKEL

DECEMBER 2001

US ARMY ARMAMENT RESEARCH,
DEVELOPMENT AND ENGINEERING CENTER
CLOSE COMBAT ARMAMENTS CENTER
BENÉT LABORATORIES
WATERVLIET, N.Y. 12189-4050

DISCLAIMER

The findings in this report are not to be construed as an official Department of the Army position unless so designated by other authorized documents.

The use of trade name(s) and/or manufacturer(s) does not constitute an official endorsement or approval.

DESTRUCTION NOTICE

For classified documents, follow the procedures in DoD 5200.22-M, Industrial Security Manual, Section II-19, or DoD 5200.1-R, Information Security Program Regulation, Chapter IX.

For unclassified, limited documents, destroy by any method that will prevent disclosure of contents or reconstruction of the document.

For unclassified, unlimited documents, destroy when the report is no longer needed. Do not return it to the originator.

REPORT DOCUMENTATION PAGE

Form Approved
OMB No. 0704-0188

1. AGENCY USE ONLY *(Leave blank)*	2. REPORT DATE	3. REPORT TYPE AND DATES COVERED
	December 2001	Final

4. TITLE AND SUBTITLE

COATING-BOND EVALUATION USING DISPERSION CURVES AND LASER-ULTRASONICS

5. FUNDING NUMBERS

AMCMS No. 6226.24.H191.1

6. AUTHOR(S)

Agostino Abbate (Panametrics, Inc., Waltham, MA),
Bryon Knight (Plug Power, Latham, NY),
Moayyed A. Hussain, Julius Frankel

7. PERFORMING ORGANIZATION NAME(S) AND ADDRESS(ES)

U.S. Army ARDEC
Benet Laboratories, AMSTA-AR-CCB-O
Watervliet, NY 12189-4050

8. PERFORMING ORGANIZATION REPORT NUMBER

ARCCB-TR-01025

9. SPONSORING / MONITORING AGENCY NAME(S) AND ADDRESS(ES)

U.S. Army ARDEC
Close Combat Armaments Center
Picatinny Arsenal, NJ 07806-5000

10. SPONSORING / MONITORING AGENCY REPORT NUMBER

11. SUPPLEMENTARY NOTES

12a. DISTRIBUTION / AVAILABILITY STATEMENT

Approved for public release; distribution unlimited.

12b. DISTRIBUTION CODE

13. ABSTRACT *(Maximum 200 words)*

The dispersion characteristics of Rayleigh surface waves are used to distinguish the quality of the bond between a coating and the metallic substrate. The velocity versus frequency curves for *good* or "*welded*" bonds differ significantly from the correspondent dispersion curves for *poorer* or "*smooth*" bonds. A theoretical dynamic model of the ultrasonic experiments was developed and compared with experimental results.

As examples of welded contacts, we used coatings of tantalum sputtered on steel, or of chromium electrodeposited on steel. As examples of smooth contacts, we used thin films of nickel and tantalum weakly bonded to copper and steel substrates, respectively. The experiments were performed using laser generation and detection of surface waves traveling along the coated surface of a flat sample. The ultrasonic waves were generated in an annular ring pattern, and the converging waves at the center of the ring were detected using an optical interferometer. Wavelet analysis was used on the acquired ultrasonic signals to obtain the experimental dispersion (velocity-frequency) curves. An analytical proof is presented herein as to their applicability for this purpose. Dispersion curves obtained from the experiment and signal processing correlate with theory for the welded contact and show features of the theory for the smooth contact.

14. SUBJECT TERMS

Rayleigh Waves, Laser-Ultrasonics, Coatings

15. NUMBER OF PAGES

26

16. PRICE CODE

17. SECURITY CLASSIFICATION OF REPORT	18. SECURITY CLASSIFICATION OF THIS PAGE	19. SECURITY CLASSIFICATION OF ABSTRACT	20. LIMITATION OF ABSTRACT
UNCLASSIFIED	UNCLASSIFIED	UNCLASSIFIED	UL

TABLE OF CONTENTS

TABLES

LIST OF ILLUSTRATIONS

ACKNOWLEDGEMENTS

We gratefully acknowledge the following personnel:

- Mr. Jeffrey Braunstein performed some of the wavelet analysis.
- Mr. Joseph F. Cox did the chromium electroplating.
- Dr. Paul J. Cote provided the sputtered tantalum specimen.

INTRODUCTION

Bond evaluation between a thin coating and the substrate is an important and subtle problem. Achenbach and Epstein (ref 1) have modeled the coating/substrate bond using the acoustic boundary conditions between the two systems. They defined two types of boundary conditions for smooth and welded bonds, respectively. The analysis presented was based on the propagation model of straight-crested Rayleigh waves. We have extended the model to account for an annular acoustic source.

Rayleigh waves are nondispersive on an uncoated surface. In general, they are dispersive when generated on the coated surface of the sample. These waves travel along the surface, and their energy is contained within a depth approximately equal to their wavelength (Figure 1). At the high frequencies the acoustic wavelength is smaller than the coating thickness, and the wave mostly propagates within the coating. As the wavelength of the wave is increased, at lower frequencies, more and more acoustic energy penetrates into the substrate material and for large enough wavelengths, the wave propagates mostly in the substrate. The interface causes interesting dispersion effects; for wavelengths close to the thickness of the coating, the effect of the interface between the coating and the substrate is maximum.

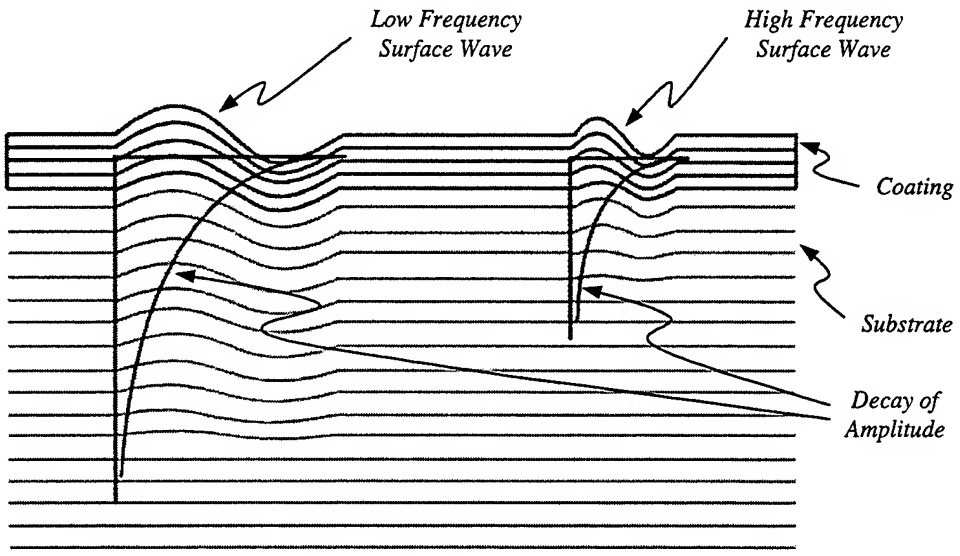

Figure 1. Schematic of surface waves of different frequencies traveling in a layered material with a welded bond.

The Rayleigh waves are generated at the surface, and their amplitude is of the order of nanometers. The coating thicknesses here are in the milli-inch range.

It turns out that the coupling of the waves between the substrate and layer is dependent on the nature of the bond, or on the boundary conditions, i.e., the conditions of stress and displacement transmittal between coating and substrate. We can define two different boundary conditions:

- Good bond between the coating and substrate (welded contact)
- Poor bond (smooth contact)

In the case of the welded contact, all the stresses and displacements are continuous across the interface. In the case of the smooth contact, the normal stresses and displacements are continuous and the shear stresses in the plane of the interface are zero. These conditions are used to theoretically calculate the phase and group velocity of the Rayleigh wave as a function of the wave's frequency. This is the so-called dispersion relation.

The results relevant to the proposed model were obtained using experiments on coated samples. Surface waves were generated on the sample using a short laser pulse, and a Michelson optical interferometer was used to detect the normal displacement of the surface at the detection point. In order to improve the signal-to-noise ratio, circularly-crested surface waves were used. The surface wave is generated in a circle, and detection is performed on the converging waves at the center of the annulus. Using this approach originally proposed by Cielo et al. (ref 2), we were able to obtain higher acoustic energy at the detection point without having to increase the generation power beyond the ablation threshold.

The validity of the resulting dispersion matrices (ref 1), which involve straight-crested waves, was not heretofore examined for the condition of annular generation. We present herein the analytic solution for circularly-crested waves converging to a point. The 6x6 matrix resulting from Achenbach and Epstein's (ref 1) solution for straight-crested waves becomes a 9x9 matrix for circularly-crested waves in our analysis. We show that the latter reduces to Achenbach and Epstein's matrix when the condition of zero torque on the surface is imposed.

In order to extract the dispersion relation from the experimental data, the signals were analyzed using wavelet signal processing. The details of this procedure and the experimental results are given below.

MODEL OF PROPAGATION ALONG A COATED SURFACE

Waves that propagate along the free surface of a semi-infinite solid travel as Rayleigh surface waves. Achenbach and Epstein (ref 1) provide a two-dimensional analysis with various boundary conditions for straight-crested *free waves* in a system consisting of layer (coating) and half space (substrate). They have solved for the dispersion relation in two dimensions, r and z. Here we solve the axisymmetric case in the coordinate system r, z, and θ, as depicted in Figure 2.

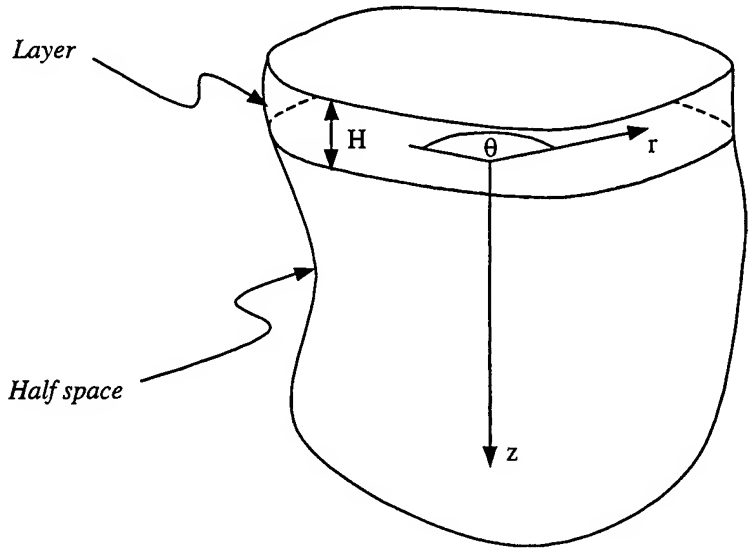

Figure 2. Schematic representation of the layer and half space model used in the theoretical calculations.

The equation of equilibrium in terms of displacements can be written as

$$(\lambda+2\mu)\nabla(\nabla\cdot\vec{u})-\mu\nabla\times(\nabla\times\vec{u})-\rho\frac{\partial^2\vec{u}}{\partial t^2}=0 \tag{1}$$

where λ and μ are the Lamé constants, ρ is the material density, and $\vec{u}$ is the displacement. Using the Helmholtz decomposition (ref 3), the displacement can be expressed using scalar and vector potentials as

$$\vec{u}=\nabla\phi+\nabla\times\vec{\psi} \tag{2}$$

with

$$\nabla\cdot\vec{\psi}=0 \tag{3}$$

It can be shown that the equation of motion can be reduced to the solutions of the following scalar and vector equations:

$$\nabla^2\vec{\psi}-\frac{1}{V_s^2}\frac{\partial^2\vec{\psi}}{\partial t^2}=0 \qquad \nabla^2\phi-\frac{1}{V_l^2}\frac{\partial^2\phi}{\partial t^2}=0 \tag{4}$$

where the shear and longitudinal bulk velocities are respectively

$$V_s^2=\frac{\mu}{\rho} \qquad V_l^2=\frac{\lambda+2\mu}{\rho} \tag{5}$$

Assuming for the time-dependence a factor of the form $e^{i\omega t}$, and depicting c as the velocity of the wave, we can define for the layer

$$q_a^2 = 1 - \frac{c^2}{V_{l_a}^2} \qquad s_a^2 = 1 - \frac{c^2}{V_{s_a}^2} \qquad k = \frac{\omega}{c} \tag{6}$$

The same equations apply for the half space by substituting b to the subscript a. The solution of equation (4) in the layer can be written as

$$\phi_a(r,z,\theta) = \left\{A_a J_0(kr)e^{-q_a kz} + L_a J_0(kr)e^{q_a kz}\right\}e^{i\omega t} \tag{7a}$$

$$\vec{\psi}_a(r,z,\theta) = \left\{\begin{array}{l}\left[B_a J_1(kr)e^{-s_a kz}, C_a J_1(kr)e^{-s_a kz}, \frac{B_a}{s_a} J_0(kr)e^{-s_a kz}\right] \\ +\left[M_a J_1(kr)e^{s_a kz}, N_a J_1(kr)e^{s_a kz}, -\frac{M_a}{s_a} J_0(kr)e^{s_a kz}\right]\end{array}\right\}e^{i\omega t} \tag{8a}$$

The solution of equation (4) in the half space is as follows:

$$\phi_b(r,z,\theta) = \left\{A_b J_0(kr)e^{-q_b kz}\right\}e^{i\omega t} \tag{7b}$$

$$\vec{\psi}_b(r,z,\theta) = \left\{\left[B_b J_1(kr)e^{-s_b kz}, C_b J_1(kr)e^{-s_b kz}, \frac{B_b}{s_b} J_0(kr)e^{-s_b kz}\right]\right\}e^{i\omega t} \tag{8b}$$

Computing the displacements from equation (2) above and using stress-strain relations for the axisymmetric case, we have the following pertinent quantities for the regions 1 and 2:

$$\begin{aligned} u_r^a &= -A_a k J_1 e^{-kq_a z} + C_a s_a k J_1 e^{-s_a kz} - L_a k J_1 e^{kq_a z} - N_a s_a k J_1 e^{s_a kz} \\ u_\theta^a &= B_a k \frac{1-s_a^2}{s_a} J_1 e^{-s_a kz} - M_a k \frac{1-s_a^2}{s_a} J_1 e^{-s_a kz} \\ u_z^a &= C_a k J_0 e^{-s_a kz} - kq_a A_a J_0 e^{-kq_a z} + N_a k J_0 e^{s_a kz} - kq_a L_a J_0 e^{kq_a z} \end{aligned} \tag{9}$$

$$\begin{aligned} u_r^b &= -A_b k J_1 e^{-kq_b z} + C_b s_b k J_1 e^{-s_b kz} \\ u_\theta^b &= B_b k \frac{1-s_b^2}{s_b} J_1 e^{-s_b kz} \\ u_z^b &= C_b k J_0 e^{-s_b kz} - kq_b A_b J_0 e^{-kq_b z} \end{aligned} \tag{10}$$

$$\sigma_z^a = \frac{A_a E_a k^2((1-\sigma_a)q_a{}^2 - \sigma_a)}{(1+\sigma_a)(1-2\sigma_a)} J_0 e^{-q_a kz} - \frac{C_a E_a s_a k^2}{(1+\sigma_a)} J_0 e^{-s_a kz}$$
$$+ \frac{L_s E_a k^2((1-\sigma_a)q_a{}^2 - \sigma_a)}{(1+\sigma_a)(1-2\sigma_a)} J_0 e^{q_1 kz} + \frac{N_a E_a s_a k^2}{(1+\sigma_a)} J_0 e^{s_a kz} \tag{11}$$

$$\tau_{rz}^a = \frac{A_a E_a k^2 q_a}{(1+\sigma_a)} J_1 e^{-q_a kz} - \frac{C_a E_a (1+s_a{}^2)k^2}{2(1+\sigma_a)} J_1 e^{-s_a kz}$$
$$- \frac{L_a E_a k^2 q_a}{(1+\sigma_a)} J_1 e^{q_a kz} - \frac{N_a E_a (1+s_a{}^2)k^2}{2(1+\sigma_a)} J_1 e^{s_a kz} \tag{12}$$

$$\tau_{\theta z}^a = -\frac{B_a E_a k^2 (1-s_a{}^2)}{2(1+\sigma_a)} J_1 e^{-s_a kz} - \frac{E_a M_a (1-s_a{}^2)k^2}{2(1+\sigma_a)} J_1 e^{s_a kz} \tag{13}$$

$$\sigma_z^b = \frac{A_b E_b k^2((1-\sigma_b)q_b{}^2 - \sigma_b)}{(1+\sigma_b)(1-2\sigma_b)} J_0 e^{-q_b kz} - \frac{C_b E_b s_b k^2}{(1+\sigma_b)} J_0 e^{-s_b kz} \tag{14}$$

$$\tau_{rz}^b = \frac{A_b E_b k^2 q_b}{(1+\sigma_b)} J_1 e^{-q_b kz} - \frac{C_b E_b (1+s_b{}^2)k^2}{2(1+\sigma_b)} J_1 e^{-s_b kz} \tag{15}$$

$$\tau_{\theta z}^b = -\frac{B_b E_b (1-s_b{}^2)k^2}{2(1+\sigma_b)} J_1 e^{-s_b kz} \tag{16}$$

The Bessel functions in the above are either $J_n(qkr)$ or $J_n(skr)$, with proper subscripts depending on the associated exponential terms.

So far the analysis has focused on plane harmonic waves with real phase velocities and wave numbers that propagate in the system of coating and substrate. The relationship between the velocity and the frequency is determined by the boundary conditions between coating and substrate. The two types of bonds discussed here impose different boundary conditions, hence result in different dispersion relations.

The boundary conditions to be imposed are functions of the bond between the layer and half space. For the *welded contact*, the boundary conditions are

$$\sigma_{z_a} = 0,\ \tau_{rz_a} = 0,\ \tau_{\theta z_a} = 0 \ at\ z = -H \tag{17}$$

$$u_{z_a} = u_{z_b},\ u_{r_a} = u_{r_b},\ u_{\theta_a} = u_{\theta_b},\ \tau_{rz_a} = \tau_{rz_b},\ \tau_{\theta z_a} = \tau_{\theta z_b},\ \sigma_{z_a} = \sigma_{z_b} \ at\ z = 0 \tag{18}$$

For the *smooth contact*, the boundary conditions are

$$\sigma_{z_a} = 0,\ \tau_{rz_a} = 0,\ \tau_{\theta z_a} = 0 \ at\ z = -H \tag{19}$$

$$u_{z_a} = u_{z_b},\ \tau_{rz_a} = 0,\ \tau_{rz_b} = 0,\ \tau_{\theta z_a} = 0,\ \tau_{\theta z_b} = 0,\ \sigma_{z_a} = \sigma_{z_b} \ at\ z = 0 \tag{20}$$

These boundary conditions lead to a set of nine homogenous equations involving geometric parameters, elastic constants, frequency, and acoustic velocity. For the solution to exist, the 9x9 determinant of homogeneous equations has to vanish. The zeros of the determinant lead to dispersion curves.

Welded Contact

In this case the determinant is given by

$$\begin{vmatrix}
\frac{1+s_a^2}{2}e^{-q_a kH} & -s_a e^{q_a kH} & \frac{1+s_a^2}{2}e^{q_a kH} & s_a e^{q_a kH} & 0 & 0 & 0 & 0 & 0 \\
2q_{a1}e^{-q_1 kH} & -(1+s_a^2)e^{-s_a kH} & -2q_a e^{q_a kH} & -(1+s_a^2)e^{s_a kH} & 0 & 0 & 0 & 0 & 0 \\
-1 & s_a & -1 & -s_a & 1 & -s_b & 0 & 0 & 0 \\
-q_a & 1 & q_a & 1 & q_b & -1 & 0 & 0 & 0 \\
\frac{1+s_a^2}{2\sigma_1} & \frac{-s_a}{\sigma_a} & \frac{1+s_a^2}{2\sigma_a} & \frac{s_a}{\sigma_a} & -\frac{(1+s_b^2)\mu_b}{2\sigma_a\mu_a} & \frac{s_b\mu_b}{\sigma_a\mu_a} & 0 & 0 & 0 \\
2q_a & -(1+s_a^2) & -2q_a & -(1+s_a^2) & -\frac{2q_b\mu_b}{\mu_a} & \frac{(1+s_b^2)\mu_b}{\mu_a} & 0 & 0 & 0 \\
0 & 0 & 0 & 0 & 0 & 0 & -e^{-s_a kH} & -e^{s_a kH} & 0 \\
0 & 0 & 0 & 0 & 0 & 0 & \frac{1-s_a^2}{s_a} & -\frac{1-s_a^2}{s_a} & -\frac{1-s_b^2}{s_b} \\
0 & 0 & 0 & 0 & 0 & 0 & -(1-s_a^2) & -(1-s_a^2) & (1-s_b^2)\frac{\mu_b}{\mu_a}
\end{vmatrix} \tag{21}$$

As already indicated, the acoustic waves generated in our tests are axisymmetric in nature. In addition torsional modes, even if generated by mode conversion, cannot be detected by the interferometer. From equation (21), the determinant can be decomposed as a product of two subdeterminants $D = D1 \bullet D2$, where $D1$ is the upper left-hand corner determinant corresponding to the nontorsion components of the wave, and $D2$ is the lower right-hand corner determinant corresponding to torsion modes. This separation can also be verified if we apply the following boundary conditions in addition to those applied for normal stresses and displacements shown in equation (20):

$$\tau_{\theta z}(z=H)=0, \quad u_\theta^a(z=0)=0, \quad u_\theta^b(z=0)=0, \quad \tau_{\theta z}^a(z=0)=0, \quad \tau_{\theta z}^b(z=0)=0 \tag{22}$$

The determinant $D1$ is given by

$$\begin{vmatrix}
\frac{1+s^2{}_a}{2}e^{-q_a kH} & -s_a e^{q_a kH} & \frac{1+s_a^2}{2}e^{q_a kH} & s_a e^{s_a kH} & 0 & 0 \\
2q_a e^{-q_a H} & -(1+s_a^2)e^{-s_a kH} & -2q_a e^{q_a kH} & -(1+s_a^2)e^{s_a kH} & 0 & 0 \\
-1 & s_a & -1 & -s_a & 1 & -s_b \\
-q_a & 1 & q_a & 1 & q_b & -1 \\
\frac{1+s_a^2}{2\sigma_a} & \frac{-s_a}{\sigma_a} & \frac{1+s_a^2}{2\sigma_a} & \frac{s_a}{\sigma_a} & -\frac{(1+s_b^2)\mu_b}{2\sigma_a\mu_a} & \frac{s_b\mu_b}{\sigma_a\mu_a} \\
2q_a & -(1+s_a^2) & -2q_a & -(1+s_a^2) & \frac{-2q_b\mu_b}{\mu_a} & \frac{(1+s_b^2)\mu_b}{\mu_a}
\end{vmatrix} \tag{23}$$

It can be shown that $D2 = 0$ corresponds to (the nondispersive) shear horizontal modes of a two-dimensional layer on an elastic foundation. The above determinant equation (23), with slight modifications, is identical to that of the plane-strain solution given by Achenbach and Epstein (ref 1). Hence the dispersion for all modes is identical to that of a planar system. To confirm this hypothesis, a series of experiments was carried out in which the dispersion curves were generated with a series of diminishing arcs vanishing to a point. It was found that the measured dispersion curves were invariant.

The contour plot for the subdeterminant D for the welded contact is shown in the top row of Figure 3 for the two possible cases in which the coating is acoustically stiffer than the substrate (left image) or the opposite (right image). Here the value of the determinant D is plotted in pseudo-color on a logarithmic scale. The (darkest) points in the frequency-velocity plane with a high density of contours represent the solutions to the modified Achenbach and Epstein (ref 1) model.

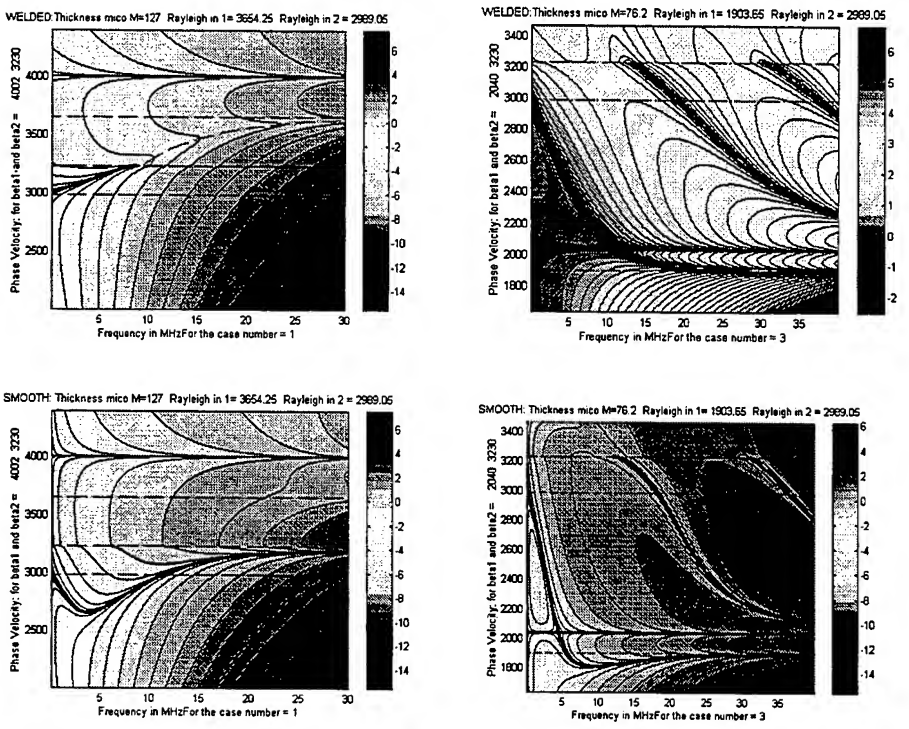

(a)

(b)

Figure 3. Theoretical phase velocity dispersion contours calculated from the experimental parameters for the following cases: coating acoustically more stiff (left) and less stiff than the substrate (right), welded contact (a), and smooth contact (b). Note: the 1 and 2 refer to the Rayleigh velocities of the layer and substrate, respectively.

Smooth Contact

For the case where the bond between the layer and substrate transmits no shear stresses or displacements (smooth contact), the boundary conditions are given in equations (19) and (20). These conditions lead to a new set of nine homogenous conditions. The determinant is given by

$$\begin{vmatrix}
\frac{1+s_a^2}{2}e^{-q_a kH} & -s_a e^{q_a kH} & \frac{1+s_a^2}{2}e^{q_a kH} & s_a e^{s_a kH} & 0 & 0 & 0 & 0 & 0 \\
2q_a e^{-q_a H} & -(1+s_a^2)e^{-s_a kH} & -2q_a e^{q_a kH} & -(1+s_a^2)e^{s_a kH} & 0 & 0 & 0 & 0 & 0 \\
-q_a & 1 & q_a & 1 & q_b & -1 & 0 & 0 & 0 \\
\frac{1+s_a^2}{2\sigma_a} & \frac{-s_a}{\sigma_a} & \frac{1+s_a^2}{2\sigma_a} & \frac{s_a}{\sigma_a} & -\frac{(1+s_b^2)\mu_b}{2\sigma_a\mu_a} & \frac{s_b\mu_b}{\sigma_a\mu_a} & 0 & 0 & 0 \\
2q_a & -(1+s_a^2) & -2q_a & -(1+s_a^2) & 0 & 0 & 0 & 0 & 0 \\
0 & 0 & 0 & 0 & -\frac{2q_b\mu_b}{\mu_b} & \frac{(1+s_b^2)\mu_b}{\mu_a} & 0 & 0 & 0 \\
0 & 0 & 0 & 0 & 0 & 0 & -e^{-s_a kH} & -e^{s_a kH} & 0 \\
0 & 0 & 0 & 0 & 0 & 0 & -(1-s_a^2) & -(1-s_a^2) & 0 \\
0 & 0 & 0 & 0 & 0 & 0 & 0 & 0 & (1-s_b^2)\frac{\mu_b}{\mu_a}
\end{vmatrix} \quad (26)$$

Again, as can be seen from above equation that the determinant can be decomposed as a product of two subdeterminants, $D = D1 \bullet D2$ where $D2$ corresponds to torsional modes and $D1$ given below is nontorsional part.

The determinant $D1$ is given by

$$\begin{vmatrix} \frac{1+s_a^2}{2} e^{-q_a kH} & -s_a e^{q_a kH} & \frac{1+s_a^2}{2} e^{q_a kH} & s_a e^{s_a kH} & 0 & 0 \\ 2q_a e^{-q_a H} & -(1+s_a^2) e^{-s_a kH} & -2q_a e^{q_a kH} & -(1+s_a^2) e^{s_a kH} & 0 & 0 \\ -q_a & 1 & q_a & 1 & q_a & -1 \\ \frac{1+s_a^2}{2\sigma_a} & \frac{-s_a}{\sigma_a} & \frac{1+s_a^2}{2\sigma_a} & \frac{s_a}{\sigma_a} & -\frac{(1+s_b^2)\mu_b}{2\sigma_a\mu_a} & \frac{s_b\mu_b}{\sigma_a\mu_a} \\ 2q_a & -(1+s_a^2) & -2q_a & -(1+s_a^2) & 0 & 0 \\ 0 & 0 & 0 & 0 & -\frac{2q_b\mu_b}{2\mu_a} & \frac{(1+s_b^2)\mu_b}{\mu_a} \end{vmatrix} \qquad (27)$$

The above determinant, with slight modifications, is identical to that for plane-strain given by Achenbach and Epstein (ref 1) for the smooth contact conditions. Hence the dispersion for all modes is identical to that of the corresponding planar system.

The contour plot for the subdeterminant D for the case of smooth contact is shown in the bottom row of Figure 3 for the two possible cases in which the coating is acoustically stiffer than the substrate (left image) or the opposite (right image). For the case of stiffer coating and welded contact, the determinant does not attain a zero but a local minimum that is between the shear velocity of the layer and the Rayleigh velocity of the coating.

The dispersion curves have been obtained from analysis using the above formulation for the cases that have been experimentally studied and are shown in Figure 4. The material properties used to generate these curves (acoustic velocities and coating thickness) were taken from values for the materials being experimentally examined. It has to be noted that the group velocity, instead of the phase velocity is presented here. The reason for this approach will be clear in the next sections, but it is linked to the need of comparing theoretical to experimental curves.

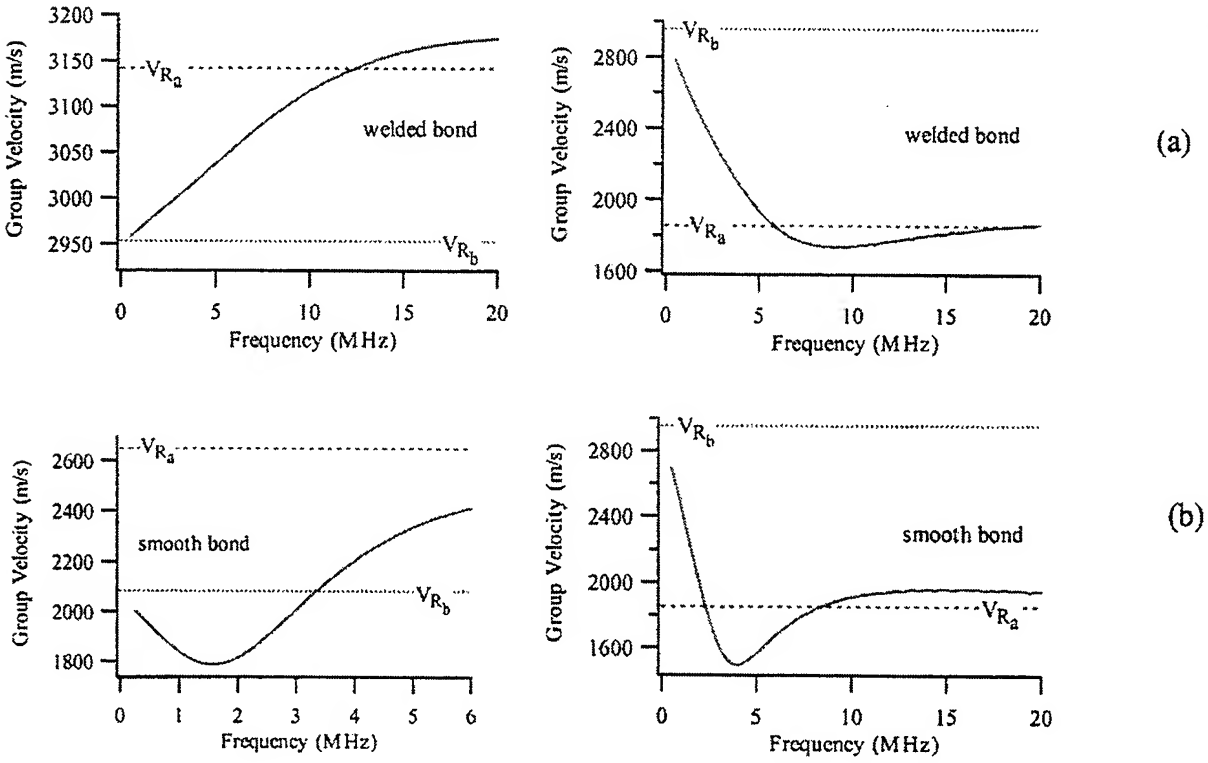

Figure 4. Theoretical dispersion curves calculated from the experimental parameters for the following cases: coating acoustically more stiff (left) and less stiff than the substrate (right); welded contact (a) and smooth contact (b). Note: VR_a and VR_b are the Rayleigh velocities of the layer and substrate, respectively.

EXPERIMENTAL DETAILS

Samples Used in This Work

The "welded" boundary condition was achieved by electrodeposition of chromium on steel and sputtering of tantalum on steel. We tried to approximate the "smooth" coupling conditions by resorting to very thin epoxy bonds for coupling acoustically "stiffer" on "softer" and "softer" on "stiffer" coating on substrate specimens (see Table 1).

Table 1. Sample Parameters

		Coating Acoustically Less Stiff Than Substrate	Coating Acoustically More Stiff Than Substrate
Welded Contact	Sample	Tantalum on Steel	Chromium on Steel
	Method	Sputtered	Electrodeposited
	Coating Thickness	0.0035 Inch	0.0036 Inch
Smooth Contact	Sample	Tantalum on Steel	Nickel on Copper
	Method	Epoxied	Epoxied
	Coating Thickness	0.005 Inch	0.005 Inch

Laser Generation and Detection of Surface Waves

A "LaserWave" system (ref 4) was used for our study. The system is illustrated in Figure 5. The Nd:YAG laser, with 532-nm wavelength, was used to generate the ultrasonic surface wave along a circle. The other parameters of interest include a 100-mJ energy/pulse and 5 to 7 nsec pulse width with a 10 Hz pulse repetition rate. Both the pulse width in time and in space contribute to the frequency content of the pulse. A Michelson interferometer is the means of detection for the surface waves at the center of the generated annulus. The HeNe detection laser provides 10 mW CW power, at a wavelength of 632.8-nm. For an isotropic surface, the waves generated at the annulus all arrive at the center at the same time. In this way, the amplitude of the surface wave is enhanced, resulting in an improved signal-to-noise ratio without ablation. In order to make the system more rugged and to simplify its operations, the Michelson interferometer arms are not temperature and vibration stabilized.

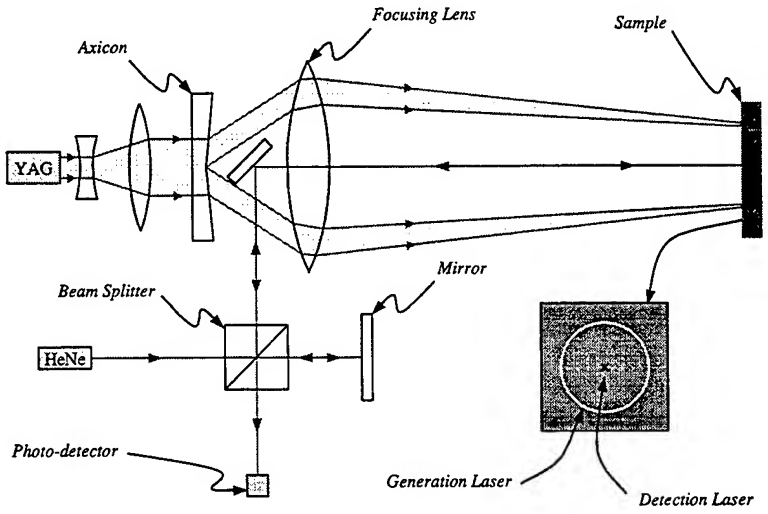

Figure 5. Schematic diagram of the pulsed laser showing annular generation with Michelson interferometer detection at the center.

A drawback to this approach is that a low frequency modulation of the optical signal is added to the ultrasonic pulse. Background vibrations of only a few micrometers will cause significant modulation in the interferometer signal, as illustrated in Figure 6. To a first-order approximation, the sensitivity of the interferometer to the ultrasonic signal is a function of the derivative of the low frequency component signal. As a result, the ultrasonic signal is multiplied by an amplification coefficient that varies between –1 and 1. Using an analog high-pass filter and a digital processing algorithm filters out this imposed modulation, due to the out-of-phase arrival of the laser radiation from the signal and reference arm.

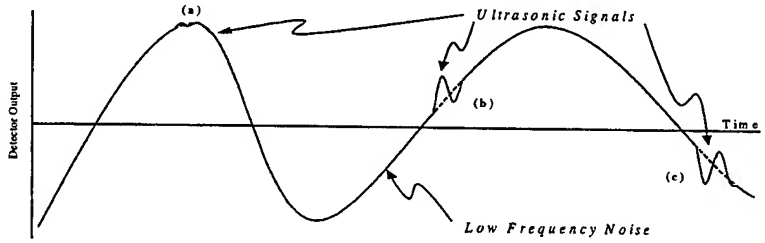

Figure 6. Ultrasonic signals (a), (b), and (c), superimposed on low frequency background noise from a nonstabilized interferometer output.

The first step in the algorithm is to filter out the low frequency modulation by using an analog high-pass filter with maximally-flat delay characteristics. The result of such an operation is shown in Figure 7. The three signals represent the different situations that can occur. Figure 7a shows the result of an ultrasonic signal detected at a point of low sensitivity (at the peak or valley of the low frequency modulation signal). In order to ensure that the signal is detected, averaging of 50 to 100 successive laser pulses is commonly utilized. Using a pulse repetition rate of 10 Hz, this results in actual measurement rates of 0.5 to 0.1 per second. Unfortunately, an added complication is that even if the sensitivity is at maximum, a 180-degree phase shift can occur, as shown in Figures 7b and 7c. Because of these phase changes, a phase compensating mechanism must be employed for effective averaging, otherwise cancellation of echoes could occur, as shown in Figure 8.

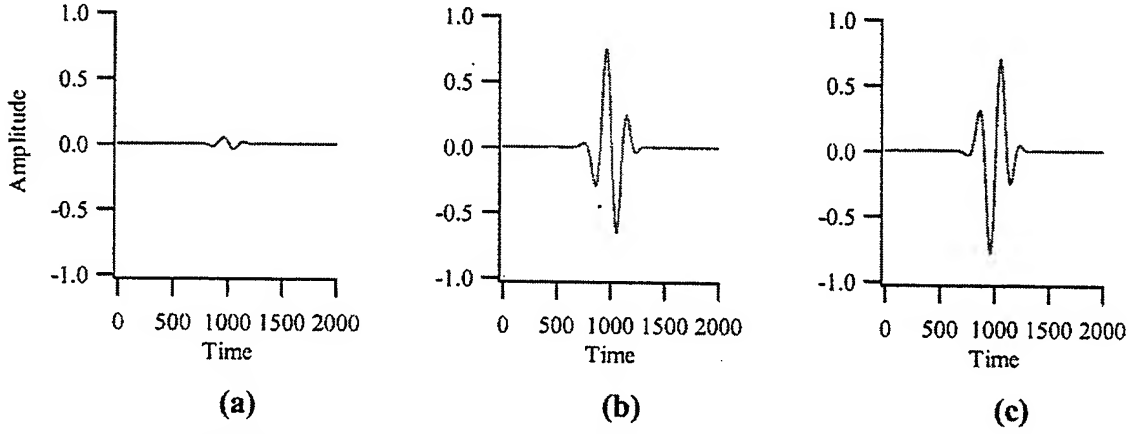

Figure 7. Ultrasonic signals (a), (b), and (c) seen in Figure 3 after filtering out low frequency noise.

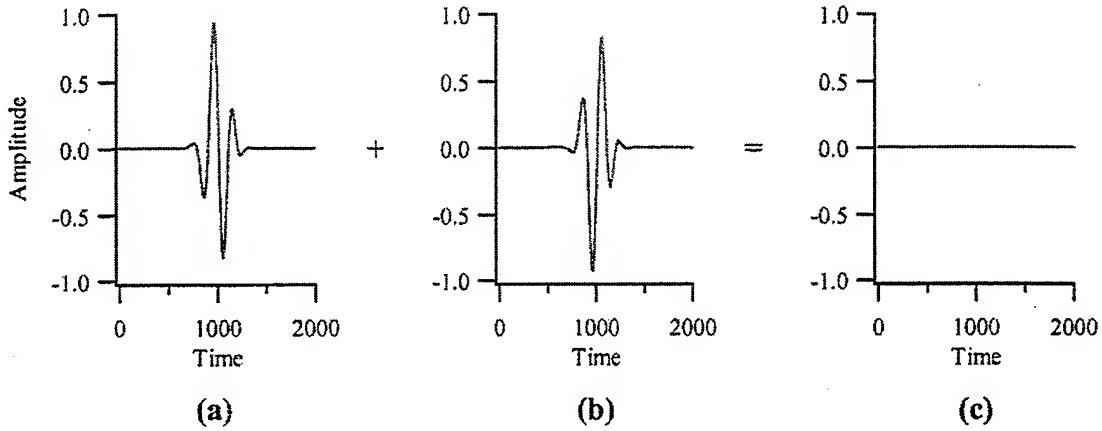

Figure 8. Demonstration of signal averaging without phase compensation. The waveform in (c) is the result of the average of the waveforms in (a) and (b).

Phase compensation (Figure 9) is thus used in conjunction with signal averaging to attain the greatest amplitude for the final signal. When two signals of opposite phase and equal amplitude, seen in Figures 8a and 8b, are averaged the result is a signal with zero amplitude, seen as Figure 8c. However, if the signal in Figure 8b is phase compensated, i.e., its phase is adjusted to match the phase of the other signal, shown in Figure 8a, the resulting average signal has the same amplitude, as seen in Figure 9c.

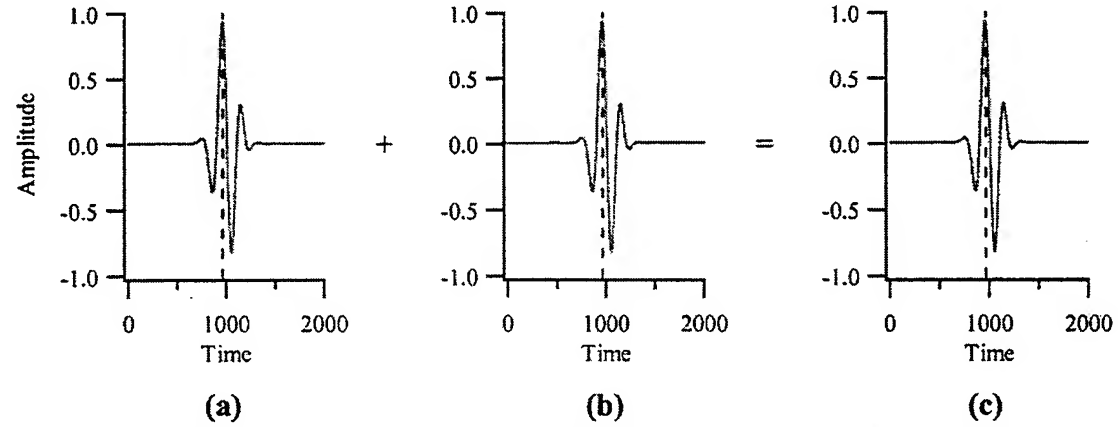

Figure 9. Demonstration of signal averaging with the use of phase compensation by selecting the point in time that corresponds to the dashed line. The waveform in (c) is the result of the average of the waveforms in (a) and (b).

The signal processing and averaging and wavelet analysis were all implemented in a LABVIEW program that will be described in a separate report.

WAVELET APPROACH TO ESTIMATE DISPERSION CURVES

From wave theory, it is known that the ultrasonic signal can be expressed as a linear combination of mono-frequency harmonic functions. The dispersion relation describes the relationship between the frequency f and the phase velocity v. For a nondispersive sample such as an uncoated substrate, the dispersion relation is constant and all the wave components travel with the same phase velocity, which in this case corresponds to the group velocity. The signal thus maintains the same shape as generated. From experiments, we have found it to be approximately Gaussian in shape. On this basis, we approximate the converging ultrasonic surface wave signal generated by an impulse laser impinging in an annulus as a set of Gaussian signals, each having its own center frequency and its own Gaussian envelope.

$$f(t)=\sum_n a_n e^{-(\frac{t-\frac{d}{V_n}}{\beta_n})^2} e^{i\omega_n(t-\frac{d}{V_n})}=\sum_n f_n(t) \tag{28}$$

where n is the number of Gaussian packets with amplitude a_n, decay parameter β_n, and center frequency ω_n. The radius of the circular annulus is d and V_n is the group velocity of the packet. For a dispersive medium V_n is a function of ω_n. d remains the same for all packets.

As previously noted, Rayleigh surface waves become dispersive in the presence of a coating layer. Since each wave component propagates with a different phase velocity, the initial shape of the transient waveform is distorted in time. By determining the time of arrival of the various wave components as a function of the frequency, the group velocity versus frequency curve can be extracted. Experimentally such dispersion gives the relation between frequency ω_n and group velocity V_n. It depends on the material properties of the coating and substrate as well as the quality of the bond. Estimation of the dispersion curve is central in characterizing the quality of the bond. Since each packet is Gaussian, a wavelet transform with a frequency modulated Gabor mother wavelet, which is also Gaussian, is thought to lead to an optimum correlation determination (ref 5).

The continuous wavelet transform of $f(t)$ is defined by (ref 5)

$$Wf(u,s)=\int_{-\infty}^{\infty} f(t)\frac{1}{\sqrt{s}}\psi^*(\frac{t-u}{s})dt \tag{29}$$

with frequency scaling s and time delay u. The modulated wavelet with a Gabor window is given by (ref 5)

$$\psi(t)=e^{i\eta t}g(t) \tag{30}$$

$$g(t)=\frac{1}{(\pi\sigma^2)^{\frac{1}{4}}}e^{\frac{t^2}{2\sigma^2}} \tag{31}$$

with center frequency η and variance of $\frac{\sigma^2}{2}$.

The Fourier transform of the wavelet is given by

$$\hat{\bar{\psi}}(\omega) = \sqrt{s}\hat{\psi}(s\omega) = (4\pi s^2\sigma^2)^{\frac{1}{4}} e^{\frac{\sigma^2}{2}(s\omega-\eta)^2} \tag{32}$$

The wavelet transform can also be expressed as a convolution integral between the signal and the wavelet and its scaled versions.

$$Wf(u,s) = \langle f(t), \psi_{us} \rangle = f * \bar{\psi}_s(u) \tag{33}$$

where

$$\bar{\psi}_s(t) = \frac{1}{\sqrt{s}}\psi^*(-\frac{t}{s}) \tag{34}$$

But convolution in the time domain is equivalent to multiplication in the frequency domain, hence using the FFT of the signal and the wavelets, the numerical integration is replaced by the dot product of two vectors leading to a fairly fast computation using MATLAB.

If the signal is expressed by a sum of Gaussian packets, as shown in equation (28), the wavelet transform can also be expressed by a sum of wavelet transforms as

$$Wf(u,s) = \sum_n Wf_n(u,s) \tag{35}$$

We can rewrite the single Gaussian packet as

$$f_n = a_n e^{-\left(\frac{(t-t_n)}{\beta_n}\right)^2} e^{j\omega_n(t-t_n)} \tag{36}$$

and its wavelet transform is calculated as

$$\begin{aligned} Wf_n(u,s) &= \langle f_n, \psi_{us} \rangle = \int_{-\infty}^{\infty} f_n(t)\frac{1}{\sqrt{s}}\psi^*(\frac{t-u}{s})dt \\ &= a_n(4\sigma^2\pi)^{\frac{1}{4}}\beta_n\frac{\sqrt{s}}{\gamma_n}e^{i\omega_n(u-t_n)}e^{i\frac{2s\sigma^2}{\gamma_n^2}(\eta-\omega_n s)(u-t_n)}e^{-\left(\frac{u-t_n}{\gamma_n}\right)^2}e^{-\left(\frac{\sigma\beta_n(\eta-\omega_n s)}{\sqrt{2}\gamma_n}\right)^2} \end{aligned} \tag{37}$$

with $\gamma_n^2 = \beta_n^2 + 2s^2\sigma^2$.

It can be shown that the wavelet transform can be used as an energy density function in the time-frequency plane. The modulus of the wavelet transform is

$$|Wf_n(u,s)| = a_n(4\sigma^2\pi)^{\frac{1}{4}}\beta_n\frac{\sqrt{s}}{\gamma_n}e^{-\left(\frac{u-t_n}{\gamma_n}\right)^2}e^{-\left(\frac{\sigma\beta_n(\eta-\omega_n s)}{\sqrt{2}\gamma_n}\right)^2} \tag{38}$$

The above expression consists of two decaying exponentials, one in the time domain and the other in the frequency domain with its maximum value at a single point given by the coordinates

$$u_n = t_n = \frac{d}{v_n} \tag{39}$$

$$\xi_n = \left(\frac{\eta}{s}\right)_n = \omega_n \tag{40}$$

The same analysis is done for each component in equations (28) and (35). The curve formed by the calculated maxima with coordinates (u_n, ξ_n) is called the ridge of the wavelet transform of the signal, and it represents the group delay versus center frequency of the various signal packets. This is the experimental dispersion curve of group delay as a function of frequency.

Once the transform is carried out, the dispersion curve becomes the locus of the ridges of the transform in the frequency-velocity plane (ref 6). As an example of this procedure, let us consider a signal composed of the sum of five different signal packets of frequencies 10, 20, 30, 40, and 50 MHz. The five signals are represented in Figure 10a. The magnitude of the correspondent wavelet transforms is plotted in Figure 10b as pseudo-color images. It can be seen that the peaks of the image of the wavelet transforms are at the right locations in frequency and time domains.

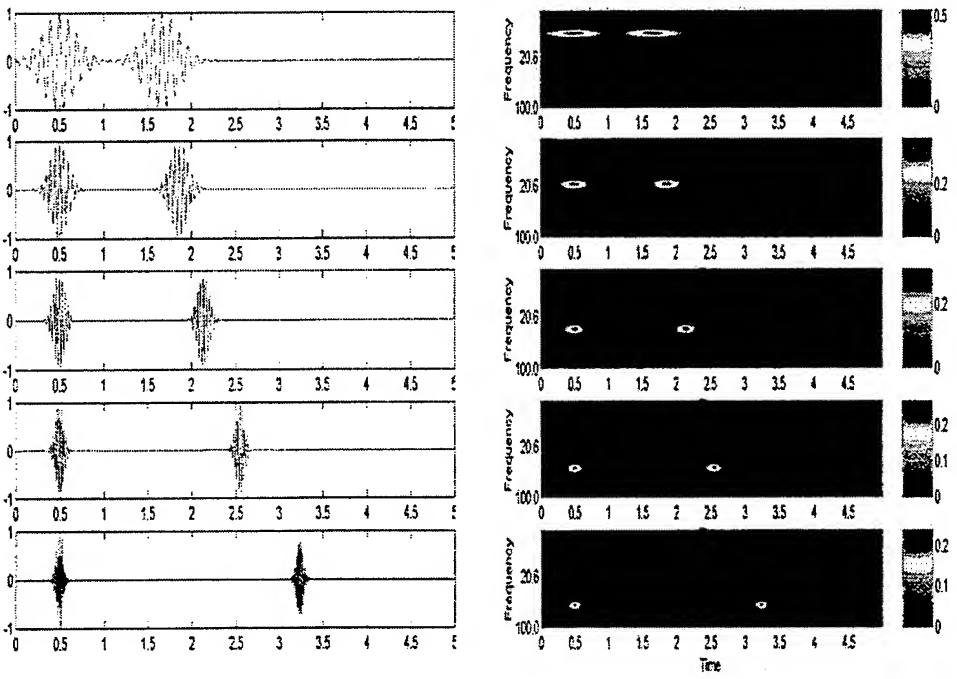

Figure 10. Signal wave packets at different frequencies and group velocities (left) and their corresponding wavelet transforms (right).

TIME-FREQUENCY RESOLUTION

The time-frequency resolution of the selected modulated Gabor wavelet depends on its time-frequency spread. $\psi(t)$ is centered at $t = 0$, therefore $\psi_{us}(t)$ is centered at $t = u$, i.e.,

$$u = \int_{-\infty}^{\infty} t\left|\psi_{us}(t)\right|^2 dt \tag{41}$$

The variance is given by

$$s^2\sigma_t^{\,2} = \int_{-\infty}^{\infty}(t-u)^2\left|\psi_{us}(t)\right|^2 dt = \frac{s^2\sigma^2}{2} \tag{42}$$

with

$$\sigma_t^{\,2} = \int_{-\infty}^{\infty}(t)^2\left|\psi(t)\right|^2 dt \tag{43}$$

The Fourier transform is given by

$$\hat{\psi}_{us}(\omega) = \sqrt{s}\hat{\psi}(s\omega)e^{-i\omega u} \tag{44}$$

with

$$\hat{\psi}(\omega) = (4\pi\sigma^2)^{\frac{1}{4}} e^{-\frac{1}{2}(\omega-\eta)^2\sigma^2} \tag{45}$$

The center frequency of the transform is defined by

$$\frac{\eta}{s} = \frac{1}{2\pi}\int_{-\infty}^{\infty}\omega|\hat{\psi}_{us}(\omega)|^2 d\omega \tag{46}$$

The energy spread of $\hat{\psi}_{us}(\omega)$ around $\frac{\eta}{s}$ is defined by

$$\frac{\sigma_\omega^{\,2}}{s^2} = \frac{1}{2\pi}\int_{-\infty}^{\infty}(\omega-\eta)^2|\hat{\psi}_{us}(\omega)|^2 dt = \frac{1}{2\sigma^2 s^2} \tag{47}$$

with

$$\sigma_\omega^{\,2} = \frac{1}{2\pi}\int_{-\infty}^{\infty}(\omega-\eta)^2|\hat{\psi}(\omega)|^2 d\omega \tag{48}$$

Dimensions of the Heisenberg box in the time and frequency domains are $s\sigma_t$ and $\frac{\sigma_\omega}{s}$ respectively, and the uncertainty is given by equality

$$\sigma_t^{\,2}\sigma_\omega^{\,2} = \frac{1}{4} \tag{49}$$

Thus the modulated Gabor Gaussians have minimum joint frequency localization and are called Gabor chirps.

RESULTS

Experimental Results

The experimental signals and their measured dispersion curves are given in Figure 11. The experimental dispersion curves in Figure 11 should be compared with the theoretical plots of Figure 4. For specifics on the specimens, please refer to Table 1.

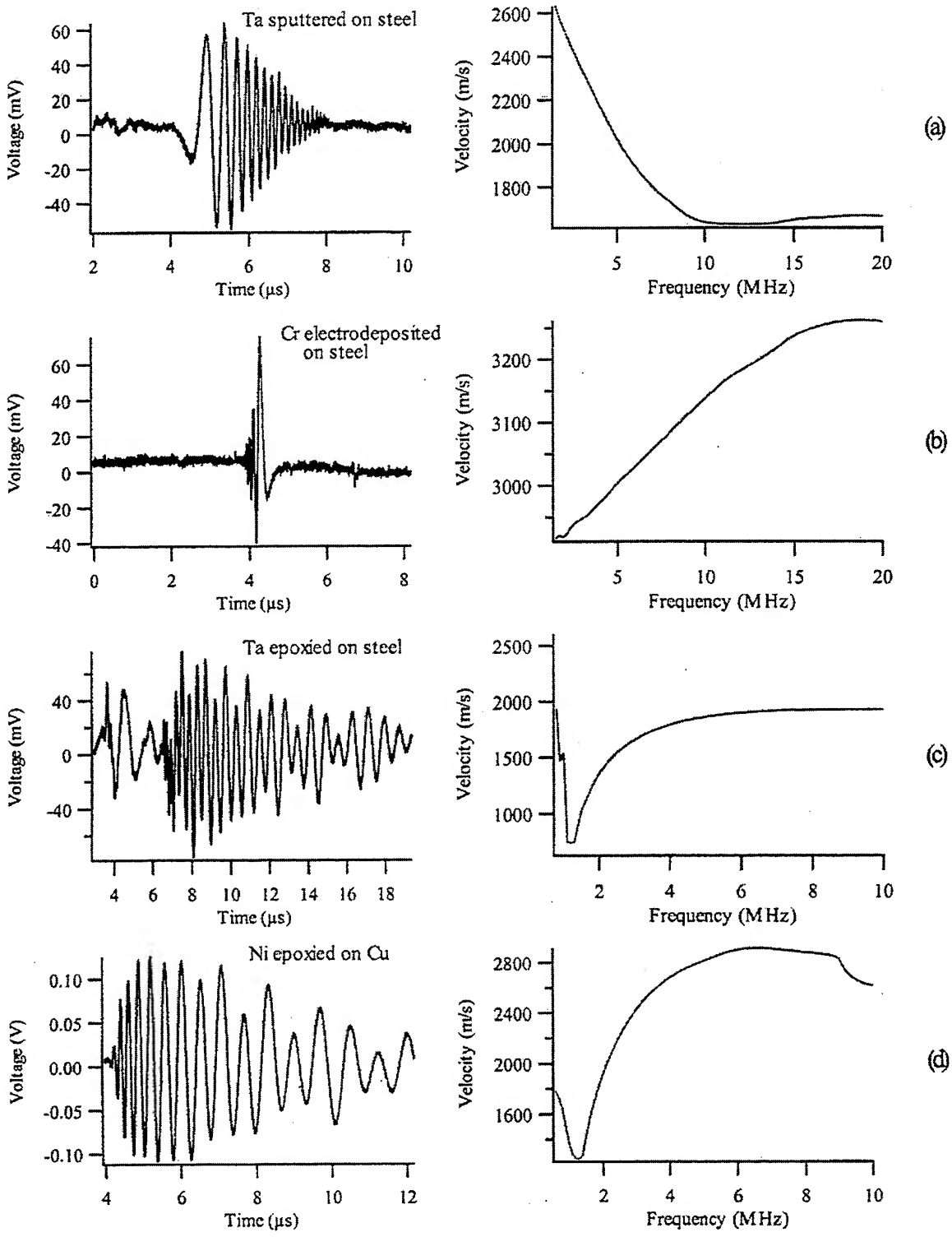

Figure 11. Waveforms from the laser-generated surface waves (left) and their corresponding dispersion curves (right).

For the "welded" coatings, tantalum on steel evinces a monotonic increase in frequency. This presents graphic experimental evidence of the results of the coupling of the Rayleigh waves across the coating interface. For the shorter wavelengths, only the tantalum velocity is exhibited; and as the wavelength is increased, the wave samples more of the substrate and the combined velocity at each frequency becomes a compromise that seems to reflect the relative coating and substrate thickness sampled, in addition to the elastic properties. For chromium electroplated on steel, the same effects are seen, but the Rayleigh velocities have the opposite relationship. Here the chromium component of the signal arrives first, since the Rayleigh velocity of the chromium is greater than that for steel.

For the epoxied coatings, which we used to simulate the "smooth" contact, we see a frequency-modulated signal in both cases. We infer that different frequencies arrive at the sensor at the same time and are superposed. Here it is more difficult to discern visually the arrival time for lower or higher frequencies, since the different frequencies "beat" against each other. This is resolved by the wavelet analysis. The location and the depth of the dip are due to the depth of penetration of the different frequencies and the material they encounter at these depths.

Analytic Results

As stated previously, we have extended Achenbach and Epstein's (ref 1) wave analysis of straight-crested surface waves for layer on half space to circularly-crested waves emanating from an annular source. We have shown that the results are similar for zero torque boundary conditions. We have also proven analytically that for Gaussian wavelets and a signal made up of Gaussian components the result of the wavelet analysis is a velocity frequency relationship for the signal.

DISCUSSION

The general aim of a work of this nature would be to differentiate nondestructively between what would empirically prove to be a good and a bad coating. This breaks down into evaluation of the bond (adhesion) and coating itself (cohesion). The determinants given in equation (23), which are for welded bonds, have been used previously to obtain thickness and elastic properties of welded coatings, with an input of only one or two other elastic properties. Regarding the bond adhesion as stated above, we took Achenbach and Epstein (ref 1) as the starting point. The ideal would have been to have an independent quantitative measure of bond quality for our coatings, even obtained destructively, and then to obtain the dispersion through our measurements. The dispersion could then be correlated with the independent test. We are still trying to find a satisfactory reference technique for evaluating or grading the quality of a bond destructively or nondestructively for our type of coating.

Achenbach and Epstein's (ref 1) suggestion of a liquid coupling between the layer and the substrate to achieve a "smooth contact" was not useful in our case, because no evidence of coating-substrate interaction could be found in the dispersion curve. Our attempts to produce electroplated chromium coatings with poor bonds also were not successful from our perspective. At present, the only way that a coating can be evaluated is through actual use. Even then all of

the coating does not react the same way. Coating failure seems to be of a statistical nature similar to fatigue failure. Some portion of the coating has a flaw, which is exacerbated through use, and which spoils its protective effect either locally or by spreading to cause more damage. Further, at present, there is a possibility that even if our dispersion curves indicated a welded bond, its adhesion could be poor. In that case, a procedure similar to a "proof" test would have to be followed. The system of coating and substrate would be subjected to substantial external stress and/or temperature pulses prior to this test. If a "welded" dispersion curve results from our tests, the bond could be said to be "good."

Several other research groups have tried to evaluate the gradation of coating quality, with free wave techniques (refs 7-12). These researchers were able to produce such gradation, each with different techniques but in each case, there were actual physical property differences in a region at and near the interface, an interlayer. Each of these research groups resorted to a three-layer analysis of the bond. The quality of the bond was tied in to the thickness of the third layer.

Four samples were measured for our experiment, as seen in Table 1, and used to simulate the welded and smooth contacts, and the slow on fast and and fast on slow conditions. Two samples were prepared by thin epoxy bonds; one was prepared by sputtering and one by electroplating. The results shown in Figure 11 indicate a satisfactory matching of the theory and experiment for the "welded" coatings and an indication of the characteristics of the smooth contact for the epoxied coating. Up to now, it was not possible for us to produce a "pure" coating-substrate combination that would test as a smooth bond. That is why we used epoxy, which acts as a third layer and approaches the smooth contact condition as the thickness decreases.

CONCLUSIONS

Rayleigh surfaces waves were generated and detected in coated materials with different bond qualities. Wavelet analysis was used to obtain dispersion curves of these signals. An analytic proof was provided as to the validity of this technique. Theoretical and experimental dispersion curves were obtained for four different cases and compared. The theoretical dispersion curves were obtained from theory based around Achenbach and Epstein (ref 1). To match our experiment, we have done the analysis for annular generation, which does not result in straight-crested waves as in Achenbach and Epstein (ref 1). However, in the absence of torsional deformation, the dispersion curves are identical to those of the straight-crested case.

As indicated in Table 1, to achieve the welded bond we used chromium electrodeposited on steel and tantalum sputtered on steel. The dispersion curves we obtained using wavelets in both cases show the shape one would expect from the analysis, with the high and low frequency values of the Rayleigh velocity corresponding to the coating and substrate, respectively, and a smooth transition between these two values at the intermediate frequencies. As Table 1 also shows, we epoxied sheets of tantalum and nickel on steel and copper, respectively. We did this to try to approximate the smooth boundary condition between layer and half space. The dispersion curves thus obtained have the approximate shape found from the analysis, but show a more pronounced dip in the low frequency region. The low frequency end of the curves gives the substrate Rayleigh velocity, whereas the higher frequency end gives the velocity for the

coating. Even the raw data from the interferometer (after averaging) indicates that a clear differentiation can be made between the welded bond of tantalum sputtered on steel and the approximation of the smooth bond obtained by the tantalum sheet epoxied to steel. The dispersion curves certainly show that difference, as well as the differences in relative stiffness between coating and substrate.

REFERENCES

1. Achenbach, J.D., and Epstein, I., "Dynamic Interaction of a Layer and a Half-Space," *Journal of Engineering Mechanics*, Proceedings of the American Society of Civil Engineers, October 1967, pp. 27-42.

2. Cielo, P., Nadeau, F., and Lamontagne, M., "Laser Generation of Convergent Acoustic Waves for Material Inspection," *Ultrasonics*, March 1985, pp. 55-62.

3. Auld, B.A., *Acoustic Fields and Waves in Solids: Vol. 2*, Krieger Publishing Company, Malabar, FL, 1990, p. 108.

4. "Laser Wave," Textron Systems Division/Subsidiary of Textron, Inc., 201 Lowell Street, Wilmington, MA 01887-2941.

5. Mallat, S., *A Wavelet Tour of Wavelet Processing*, Academic Press, 1988.

6. Abbate, A., Klimek, D., Kotidis, P., and Anthony, B., "Analysis of Dispersive Ultrasonic Signals by the Ridges of the Analytic Wavelet Transform," *Review of Progress in Quantitative Nondestructive Evaluation*, Vol. 18, (D.O. Thompson and D.E. Chimenti, Eds.), Kluwer Academic/Plenum Publishers, 1999, pp. 703-710.

7. Nagy, P.B., and Adler, L., "Ultrasonic NDE of Solid State Bonds: Inertia and Friction Welds," *Journal of Nondestructive Evaluation*, Vol. 7, No. 3/4, pp. 199-215.

8. Adler, L., Billy, M., Quentin, G., Talmant, M., and Nagy, P.B., "Generalized Lamb Modes in Friction Welded Steel Layer on Aluminum," *Review of Progress in Quantitative Nondestructive Evaluation*, Vol. 8B, pp. 1973-1980.

9. Adler, L., Billy, M., Quentin, G., Talmant, M., and Nagy, P.B., "Evaluation of Friction-Welded Aluminum-Steel Bonds Using Dispersive Guided Modes of a Layer Substrate," *Journal of Applied Physics*, Vol. 68, No. 12, December 1990, pp. 6072-6076.

10. Wu, T.T., and Chen, Y.Y., "Wavelet Analysis of Laser-Generated Surface Waves in a Layered Structure with Unbond Regions," *Journal of Applied Mechanics*, Vol. 66, June 1999, pp. 507-513.

11. Wu, T.T., and Liu, Y.H., "Inverse Determination of Thickness and Elastic Properties of a Bonding Layer Using Laser-Generated Surface Waves," *Ultrasonics*, Vol. 37, 1999, pp. 23-30.

12. Rose, J.L., Pilarski, A., Rajana, K., and Ditri, J.J., "Influence of Generation and Reception of Ultrasonic Lamb Type Plate Waves," *Review of Progress in Quantitative Nondestructive Evaluation*, Vol. 13, (D.O. Thompson et al., Eds.), pp. 1903-1910.

TECHNICAL REPORT INTERNAL DISTRIBUTION LIST

	NO. OF COPIES
TECHNICAL LIBRARY ATTN: AMSTA-AR-CCB-O	5
TECHNICAL PUBLICATIONS & EDITING SECTION ATTN: AMSTA-AR-CCB-O	3
OPERATIONS DIRECTORATE ATTN: SIOWV-ODP-P	1
DIRECTOR, PROCUREMENT & CONTRACTING DIRECTORATE ATTN: SIOWV-PP	1
DIRECTOR, PRODUCT ASSURANCE & TEST DIRECTORATE ATTN: SIOWV-QA	1

NOTE: PLEASE NOTIFY DIRECTOR, BENÉT LABORATORIES, ATTN: AMSTA-AR-CCB-O OF ADDRESS CHANGES.

TECHNICAL REPORT EXTERNAL DISTRIBUTION LIST

	NO. OF COPIES
DEFENSE TECHNICAL INFO CENTER ATTN: DTIC-OCA (ACQUISITIONS) 8725 JOHN J. KINGMAN ROAD STE 0944 FT. BELVOIR, VA 22060-6218	2
COMMANDER U.S. ARMY ARDEC ATTN: AMSTA-AR-WEE, BLDG. 3022	1
AMSTA-AR-AET-O, BLDG. 183	1
AMSTA-AR-FSA, BLDG. 61	1
AMSTA-AR-FSX	1
AMSTA-AR-FSA-M, BLDG. 61 SO	1
AMSTA-AR-WEL-TL, BLDG. 59 PICATINNY ARSENAL, NJ 07806-5000	2
DIRECTOR U.S. ARMY RESEARCH LABORATORY ATTN: AMSRL-DD-T, BLDG. 305 ABERDEEN PROVING GROUND, MD 21005-5066	1
DIRECTOR U.S. ARMY RESEARCH LABORATORY ATTN: AMSRL-WM-MB (DR. B. BURNS) ABERDEEN PROVING GROUND, MD 21005-5066	1
COMMANDER U.S. ARMY RESEARCH OFFICE ATTN: TECHNICAL LIBRARIAN P.O. BOX 12211 4300 S. MIAMI BOULEVARD RESEARCH TRIANGLE PARK, NC 27709-2211	1
COMMANDER ROCK ISLAND ARSENAL ATTN: SIORI-SEM-L ROCK ISLAND, IL 61299-5001	1
COMMANDER U.S. ARMY TANK-AUTMV R&D COMMAND ATTN: AMSTA-DDL (TECH LIBRARY) WARREN, MI 48397-5000	1
COMMANDER U.S. MILITARY ACADEMY ATTN: DEPT OF CIVIL & MECH ENGR WEST POINT, NY 10966-1792	1
U.S. ARMY AVIATION AND MISSILE COM REDSTONE SCIENTIFIC INFO CENTER ATTN: AMSAM-RD-OB-R (DOCUMENTS) REDSTONE ARSENAL, AL 35898-5000	2
COMMANDER U.S. ARMY FOREIGN SCI & TECH CENTER ATTN: DRXST-SD 220 7TH STREET, N.E. CHARLOTTESVILLE, VA 22901	1

NOTE: PLEASE NOTIFY COMMANDER, ARMAMENT RESEARCH, DEVELOPMENT, AND ENGINEERING CENTER, BENÉT LABORATORIES, CCAC, U.S. ARMY TANK-AUTOMOTIVE AND ARMAMENTS COMMAND, AMSTA-AR-CCB-O, WATERVLIET, NY 12189-4050 OF ADDRESS CHANGES.